Tetrahedral DNA mediated direct quantification of exosomes by contact-electrification effect

Peng Miao [a], Xiaoyi Ma [a], Lingjie Xie [c], Yuguo Tang [a], Xuhui Sun [c], Zhen Wen [c,*], Zhonglin Wang [b,d,**]

[a] *Suzhou Institute of Biomedical Engineering and Technology, Chinese Academy of Sciences, Suzhou 215163, China*
[b] *Beijing Institute of Nanoenergy and Nanosystems, Chinese Academy of Sciences, Beijing 100083, China*
[c] *Institute of Functional Nano and Soft Materials (FUNSOM), Jiangsu Key Laboratory for Carbon-Based Functional Materials and Devices, Soochow University, Suzhou 215123, China*
[d] *School of Material Science and Engineering, Georgia Institute of Technology, Atlanta, GA 30332–0245, United States*

ABSTRACT

Exosomes are membrane-enclosed extracellular vesicles carrying multiple biomolecules for intercellular communications. Accurate detection of exosomes could provide critical clinical information and show great significance for early diagnosis and personalized therapy of cancer. In this work, we propose a triboelectric sensing strategy for direct quantification of exosomes based on the contact-electrification effect. The target exosomes can be selectively captured on the three-dimensional tetrahedral DNA (TDNA) monolayer. The electrons transfer between abundant amino groups from exosomes and the tribo-materials contribute to the measured signal. Due to the specific output characteristic, it is able to directly discriminate 3 exosomes /μL with a linear range from 20 to 1000 exosomes/μL, even without any signal amplification. The challenges for distinguishing different cell line-derived exosomes and anti-interference in complicated biological serum systems show good performances. The presence of target exosomes can also be easily determined by visual observation of LED lighted by the generated electric energy. The proposed method can be used as a powerful tool for ultrasensitive analysis of exosomes, which is expected to have broad biological and analytical applications.

1. Introduction

Exosomes are endocytic-oriented membrane vesicles with diameters ranging from 30 to 150 nm [1], which may serve as important regulatory agents for intercellular communications [2]. Exosomes are produced by almost all kinds of cells in physiological and pathological conditions. The abundant inclusions like nucleic acids, proteins and lipids depend on the parental cells [3]. Exosomes are important information and material carriers for the communication between parental and recipient cells [4]. They may be involved in many fundamental physiological processes like neuronal communication [5], immune response [6], organ development [7], tumorigenesis [8], and metastasis [9]. However, the physiological purpose of the exosomes production still remains largely unclear and functions or applications of exosomes need continuous investigation. For example, Keller et al. discovered decoy exosomes provided protection against bacterial toxins [10]. Choi et al. engineered

an exosome-based system for drug delivery [11]. All these studies require accurate quantification of exosome concentration. Particularly, considering their significant roles in indicating disease-related physiological status, exosomes with high stability and capability of representing parental cells have been regarded as promising invasive biomarkers for the diagnosis of diseases like cancers [12]. Development of sensitive recognition and quantification method is in high demand for biological researches and clinical diagnosis [13–16].
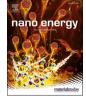
However, due to the small size of exosomes, convenient analysis of exosomes remains challenging. It is difficult to count exosomes under optical microscopy due to Abbe diffraction limit. Commonly applied flow cytometry does not perform well by weak light scattering. Standard characterization method for exosomes is the negative staining and electron microscopic visualization [17]. Nevertheless, the complicated procedure and expensive instrument limit the broad applications. Another technique for exosomes assay is nanoparticle tracking analysis

---

* Corresponding author.
** Corresponding author at: Beijing Institute of Nanoenergy and Nanosystems, Chinese Academy of Sciences, Beijing 100083, China.
E-mail addresses: wenzhen2011@suda.edu.cn (Z. Wen), zhong.wang@mse.gatech.edu (Z. Wang).

(NTA), which requires complicated isolation/purification process [18]. Worse still, NTA only reports particle size and could not specially distinguish exosomes from other interfering particles like protein aggregates. Moreover, the concentration of exosomes secreted in early stage of diseases is always quite low, which requires more sensitive methods. Therefore, the development of a highly sensitive and selective exosome detection method avoiding separation procedure is in urgent requirement.

Triboelectric nanogenerator (TENG) is a representative mechanical energy converter with low cost and simple structure [19]. Based on coupling effect between triboelectrification and electrostatic induction [20], TENG has already been widely used in various fields [21,22]. Particularly, the electrical output is critically determined by the layer adsorbed on the electrically active surface. By detailed engineering the reactions on the surface, it has great potential to be integrated into sensors or biosensors (e.g., dopamine, phenol and thrombin) with sensitive, rapid and simple in-field analysis capabilities [23–25]. In this work, we have constructed the first set of a layer of three-dimensional (3-D) DNA nanostructures on the electrically active surface for triboelectric sensing. DNA nanostructures and intermolecular interactions are particularly amenable to the synthesis of complex molecular structures [26]. Tetrahedral DNA (TDNA) is a typical 3-D DNA nanostructure with mechanical rigidity and structural stability. It could be formed by annealing of several single-stranded DNA probes, which comprise six edges of the tetrahedron [27]. In addition, three vertices of the tetrahedron could be modified with triple thiols to facilitate firm immobilization on the gold surface. The efficiency of DNA layer construction is much better than single thiol assisted immobilization, which is also well aligned with controlled density and orientation [28]. In addition, regular procedure of occupation molecule incubation can be waived. A single-stranded sequence is left on top of TDNA, which is designed as the aptamer (oligonucleotide that binds to a specific target molecule) to capture target exosomes [29]. The variation of electrical signals generated by TENG could be used to indicate the level of exosomes. The constructed TDNA layer could not only improve the specificity and efficiency for the capture of target [30], but also reflects negligible TENG background signals. Therefore, based on the designed 3-D DNA nanostructure, we have developed a fantastic triboelectric sensor for the first time to direct quantify exosome concentrations, which may also stimulate further DNA nanostructures-based TENG designs.

2. Experimental

2.1. Materials and instruments

Trisodium citrate, tris (2-carboxyethyl)-phosphine hydrochloride (TCEP), silver nitrate (AgNO$_3$), and sodium borohydride (NaBH$_4$) were purchased from Sigma (USA). Dulbecco's Modified Eagle's medium (DMEM) was purchased from Gibco (Gaithersburg, USA). Fetal bovine serum (FBS) was obtained from Hangzhou Sijiqing Biological Engineering Material Co., Ltd. (Hangzhou, China). All DNA sequences used in this work were synthesized and purified by Sangon Biotechnology Co., Ltd. (Shanghai, China). The detailed sequences and modifications were listed in Table S1. 20 bp DNA ladder was obtained from Takara Biotechnology Co., Ltd. (Dalian, China). Other reagents were of analytical grade without further purification. Ultrapure water (18 MΩ·cm) used in this work was purified by a Millipore water purification system. Ultracentrifuge Optima L-100XP (Beckman Coulter, USA) was used to separate exosomes. Transmission electron microscopy (TEM) image was taken by a JEM-1200EX transmission electron microscopy (JEOL Ltd., Japan). The concentration and diameter of the extracted exosomes were analyzed by the NanoSight LM10 (Malvern Instruments, UK) and Zetasizer Nano ZS90 (Malvern Instruments, UK), respectively. Electrochemical experiments were carried out on a CHI 660D electrochemical workstation (CH Instruments, China). The electrical outputs of the TENG were measured via a commercial linear mechanical motor

(Winnemotor, WMUC512075–06-X). The programmable electrometer (Keithley model 6514) was used to collect the open-circuit voltage (V_{oc}) and transferred charge (Q_{tr}).

2.2. Extraction and characterizations of exosomes

HeLa cells were cultured in DMEM supplemented with 10% FBS at 37 °C in 5% CO$_2$ atmosphere. After reached a confluency over 80%, the cells were washed for three times with phosphate buffer solution (PBS) and then incubated in FBS-free DMEM for another 48 h. The supernatant was then collected for the extraction of exosomes. Generally, it was centrifuged at 2000 g for 20 min and then at 10,000 g for 30 min to remove dead cells and cell debris, respectively. Subsequently, the supernatant was further centrifuged at 110,000 g for 2 h to obtain the precipitated exosomes, which were resuspended in 1 mL of PBS and stored at − 80 °C until use. The collected exosomes were firstly analyzed by negative staining TEM using a 2% solution of phosphotungstic acid. Briefly, 10 μL of exosome solution was dropped onto carbon-coated copper grids for 3 min, then excess fluid was blotted gently by filter paper from the edge. After rinsed with PBS, phosphotungstic acid solution was dropped and adsorbed onto the grids. After removing the stain, the prepared copper grids were dried at room temperature and imaged by TEM. The Nanosight instrument was then used to analyze the concentration of obtained exosomes via a laser source to illuminate the nanoparticle suspension. The Brownian motion of exosomes with scattered light can be clearly observed. In addition, Zetasizer instrument was used to measure the diameter of exosomes.

2.3. Formation and gel characterization of TDNA

TDNA was constructed by the hybridization of several single-stranded DNA probes. Each strand was firstly dissolved in the 10 mM PBS containing 0.25 M NaCl (pH 7.4). The fuel strands with equal volumes were then mixed. The resulted solution was heated to 95 °C for 5 min, and then cooled to room temperature slowly. Polyacrylamide gel electrophoresis was performed to verify the successful formation of TDNA, which was carried out in the solution (89 mM Tris-boric acid, 2 mM EDTA, pH 8.0) at 100 V for about 1 h. Afterwards, the gel was stained with 4S Red Plus, which was then photographed under UV light by Gel DocTM XR+ Imaging System (Bio-Rad, USA).

2.4. Electrochemical analysis of exosomes

A three-electrode system was applied, including an Ag/AgCl reference electrode, a platinum auxiliary electrode and a modified gold working electrode. The gold electrode was firstly cleaned. Next, the TDNA formed by probe A1, B, C, D, and E with the concentration of 1 μM was casted on the electrode surface for 8 h. The electrode was then treated with exosomes at room temperature for 1 h. Cyclic voltammetry (CV) and electrochemical impedance spectroscopy (EIS) were carried out in 5 mM [Fe(CN)$_6$]$^{3−/4−}$ with 1 M KNO$_3$. Silver nanoparticles (AgNPs) was synthesized by the borohydride reduction of AgNO$_3$. Before performed with linear sweep voltammetry (LSV) in the electrolyte of 0.1 M KCl, the TDNA modified electrode was soaked completely into 50 μL AgNPs for 20 min

2.5. Fabrication of the triboelectric sensor

A vertical contact-separation mode triboelectric sensor device was developed as follows. The top part was fabricated by the copper foil and fluorinated ethylene propylene (FEP) film into 1 × 1 cm^2, which was cohered with Kapton double-sided tape. The bottom part was the exosomes modified silicon wafer with gold film. Briefly, the silicon wafer was firstly ultrasonicated with acetone, isopropanol and ultrapure water, respectively. Then, it was treated with oxygen plasma. A gold film (100 nm) was deposited by E-Beam Evaporation on the (100) silicon

wafer (0.002–0.004 Ω·cm, 500 μm) with the unique size of 1×1 cm^2 for further use. TDNA was formed by probe A2, B, C, D according to the procedure described above. 30 μL of TDNA was dripped on the wafer overnight. After rinsed with ultrapure water, 30 μL of exosomes was dripped and the incubation lasted for 3 h. Subsequently, the wafer was rinsed with ultrapure water to remove impurities. For the electrical output measurements of the triboelectric sensor, an external tapping force was applied by a commercial linear mechanical motor. The programmable electrometer was used to test the V_{oc} and Q_{tr}. During the simulation process of the linear motor, the maximum distance between the two parts of triboelectric sensor was 5 cm, and the frequency of simulation was kept at 1.5 Hz.

2.6. Scanning Kelvin probe microscopy (SKPM) characterizations

SKPM was performed using Cypher S with Ti/Pt (5/20)-coated silicon tips (tip radius, 28 +/−10 nm; force constant, 2 N·m^{-1}; resonance frequency, 70 kHz). 2×2 μm^2 size SKPM images were scanned at a speed of 0.3 Hz, and set at a point of 50 nm from a sample in atmospheric pressure at room temperature.

2.7. Practical sample investigation

Human serum samples were supplied by local hospital (Suzhou, China). Informed written consent from all participants was obtained prior to the research. All protocols involving human subjects were previously approved by the Ethics Committee for the Use of Human Subjects of the Affiliated Suzhou Science & Technology Town Hospital of Nanjing Medical University and Suzhou Institute of Biomedical Engineering and Technology (YFE0132300). The collected serum samples were firstly centrifuged at 10, 000 g for 2 h at 4 °C. The supernatants were then treated with 0.22 μm filters, which were further diluted using PBS. Next, different amounts of isolated exosomes were spiked into the 10% serum samples before further measurements.

3. Results and discussions

3.1. Characterization and electrochemical analysis of exosomes

Exosomes are extracted and isolated by ultracentrifugation procedure. NTA results indicate the concentration of particles sized between 30 and 150 nm is 2.3×10^6 particles/mL (Fig. S1A). Saucer-like morphology is exhibited in the TEM image, which also falls in expected range (Fig. S1B). The size is further characterized by dynamic light scattering (DLS). Detailed information is listed in Fig. S1C, which is in good accordance with that of NTA and TEM results. In order to confirm the TDNA immobilization and subsequent exosome capture event on gold surface, we have firstly studied the electrochemical responses and an electrochemical sensor is developed for comparison. LSV response of synthesized AgNPs is used as the quantitative electrochemical signal [31]. The working mechanism is as illustrated (Fig. S2). Briefly, the bottomed scaffold of TDNA is firstly formed by probes A1, B, C, and D, which supports a single-stranded sequence modified with amino group in the upright orientation to absorb AgNPs via silver-amino chemistry. The successful demonstration of the interaction could be evidenced in the UV absorbance spectra. After incubating probe A1 with AgNPs, the precipitate product is resuspended and reflects a significant peak around 260 nm, which is ascribed to the attached DNA. However, in the case of probe A0 without amino group, no additional peak can be found, indicating necessity of amino group for the absorption of AgNPs (Fig. S3A). Aptamers are DNA or RNA probes, which are appealing alternatives to antibodies for the special recognition of target molecules with high binding affinity [32]. Several exosomal membrane molecules can be applied as targets including CD9, CD63, CD81, and epithelial cell adhesion molecule (EpCAM) [33,34]. Among them, CD63 is a common protein and its aptamer sequence is selected for specific recognition [35,

36]. Since probe E (aptamer sequence) contains complementary sequence with the single-stranded DNA sequence on top of TDNA, the amino group is hidden after the hybridization reaction and can no longer interact with AgNPs. As a result, the sharp silver stripping peak current disappears, which is similar to the TDNA modified electrode without NH$_2$ for capture (Fig. S3B). Nevertheless, in the presence of exosome, it could be specially recognized by probe E and the double-stranded structure is destroyed with the gain in configurational entropy. As a result, amino group is exposed for the capture of AgNPs. By analyzing the increased LSV responses, the existence of exosomes could be determined. In addition, to demonstrate the specificity of the aptamer, we have employed a range of potential interfering proteins in the electrochemical system including mucin 1 (MUC1), alpha-fetoprotein (AFP), carcinoembryonic antigen (CEA), bovine serum albumin (BSA) and hemoglobin. After reacting with these proteins, the finally obtained LSV peaks are still negligible compared with target exosome, which verify the high selectivity owing to the applied aptamer (Fig. S3C).

The electrochemical properties after surface modification are studied. We have firstly incubated the gold electrode with the five DNA probes, separately. Only in the presence of probe B, C, D with thiols modifications, CV peaks drop significantly due to the repellant between the immobilized negatively charged DNA and [Fe(CN)$_6$]$^{3-/4-}$. The other probes cannot specially interact with a gold surface, thus the CV responses are comparable with blank case (Fig. S4A). EIS results further demonstrate the conclusion (Fig. S4B). Only with thiol modified DNA probes, the modified electrodes show much larger interfacial charge transfer resistances. We have then compared the EIS and CV performances after the modification of 3-D TDNA. In a typical nyquist diagram, the semicircle diameter is the reflection of charge transfer resistance. After the modification with TDNA, a large semicircle is observed. However, after adding exosomes, the diameter of the semicircle gets smaller and the charge transfer resistance is decreased, which is due to the release of probe E from the TDNA by the interaction between exosome and its aptamer sequence (Fig. S4C). On the other hand, CV observations support the feasibility of the electrochemical system for exosome detection (Fig. S4D). In addition, we have calculated the density of TDNA on the gold surface by performing chronocoulometry measurements. According to the formula: $\Gamma = Q/nFA$ (Γ: surface coverage of electrochemical species, A: the area of the gold surface, Q: area of the oxidation peak or reduction peak in CV, n: the number of electrons transferred, F: Faraday constant), the surface coverage of TDNA is quantified to be 1.23 pmol/cm^2, which is suitable for exosome capture. Quantitative electrochemical analysis of exosomes is then carried out by performing LSV. The level of exosome determines the amount of attached AgNPs for the highly characteristic solid-state reaction. The corresponding stripping peaks are shown in Fig. S4E. Detailed relationship between the peak current and exosome concentration is summarized in Fig. S4F. A linear equation is fitted as follows:

$$y = 0.257 + 0.00109\ x\ (n = 3,\ R^2 = 0.987) \tag{1}$$

where y stands for the peak current (μA), and x is the concentration of exosomes (/μL). The limit of detection (LOD) is calculated to be 20 exosomes/μL.

3.2. Feasibility investigation of triboelectric sensing strategy

Besides traditionally electrochemical system, herein we have fabricated a label-free triboelectric sensor for exosome assay. The driving force for the triboelectrification process is based on the chemical potential difference between two contact layers, which can be significantly influenced by the captured exosome layer on one contact surface. In this place, the aptamer sequence is integrated into the TDNA nanostructure (probe A2), which not only simplifies the experimental operations, but also achieves "signal-on" mode. The prepared TDNA is firstly constructed by hybridization between the four single-stranded DNA probes,

the process of which could be confirmed by the sizes observed in the polyacrylamide gel electrophoresis image (Fig. S5A) [37]. The yield of TDNA is about 50% according to our previous study [38]. As illustrated in Fig. 1A, TDNA is then immobilized on the gold film coated silicon wafer with an optimized concentration of 5 μM (Fig. S5B). Subsequently, the exosomes in the samples to be tested could be specially captured by the aptamer sequence on top of the TDNA. Fig. 1B shows the detailed sensing mechanism driven by contact electrification and electrostatic induction. The layer of TDNA with captured exosomes is the bottom contact surface while FEP layer is the top contact surface. As known, DNA is composed of nucleotides which contain phosphoric acids, riboses and bases; meanwhile, various proteins made up of different amino acids are distributed on the surface of exosomes. Amino groups in the bases and amino acids tend to lose electrons, providing additional charges

from molecular polarizations [39]. On the contrary, FEP possess the highest electron affinity, which is the most suitable negative contact layer for TENG. When the two layers are pressed into contact, electrons are transferred to FEP and positive charges are generated on the bottom surface. With the electric potential difference, an alternating current signal in external circuit could be generated with a periodical contact-separation process. Since the charge transfer is closely related to the amount of amino groups that lose electrons [40], the concentration of initial exosomes could be estimated. The application of TENG also eliminates possible influence of exosomes shapes on detection results. Theoretically, one exosome could be captured by one or more aptamers on TDNA layer, and the TENG signal variation is mainly determined by amino group number on the surface. Compared with exosomes, TDNA contributes to limited number of lost electrons. Thus, output TENG
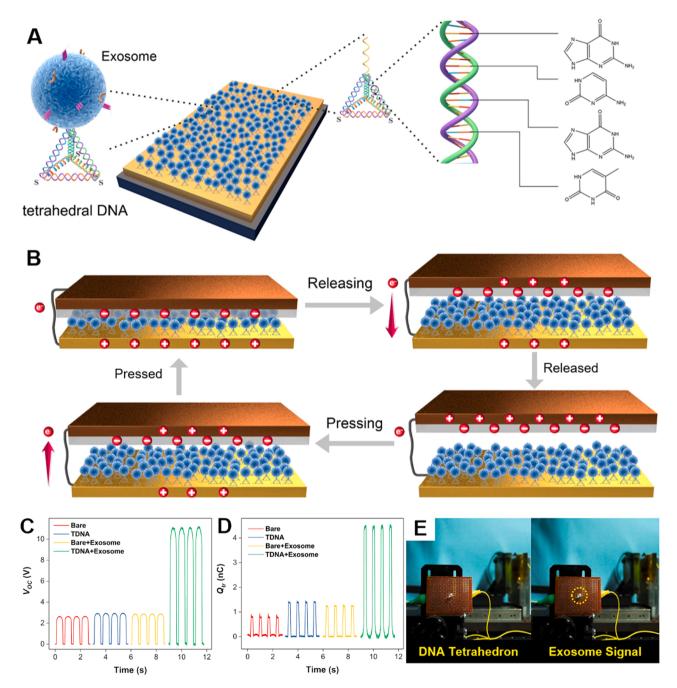

Fig. 1. Illustrations of the triboelectric sensor for direct quantification of exosomes. (A) Scheme of contact-electrification detection of exosomes. (B) Triboelectric generation mechanism for the sensor. (C) V_{oc} and (D) Q_{tr} of bare gold and TDNA based triboelectric sensor in the absence and presence of exosomes. (E) Demonstration of qualitative analysis. The concentration of exosome used is 1000 /μL.

signal is less significant compared with the captured exosomes. We have studied the performances of the fabricated triboelectric sensor (1 cm^2 in contact), which are mechanically triggered by a linear motor at 1.5 Hz. The parameters of V_{oc} and Q_{tr} are measured and compared. As shown in Fig. 1C, V_{oc} of TDNA modified wafer behaves nearly the same as bare wafer. However, after the capture of exosomes, significant increase of V_{oc} is observed. On the other hand, in the absence of TDNA layer, the signal change disappears, demonstrating the recognition element of TDNA is crucial to capture exosomes. Similar trends can be found for the parameters of Q_{tr} (Fig. 1D). We have then preliminarily employed LED to indicate the existence of target. The LED could be lighted with a certain intensity depending on the concentration of exosomes (Fig. 1E), which could be observed more clearly in Supporting Video S1. There results demonstrate the feasibility of the triboelectric sensor for exosome assay.

Supplementary material related to this article can be found online at doi:10.1016/j.nanoen.2021.106781.

3.3. Quantitative analysis using the triboelectric sensor
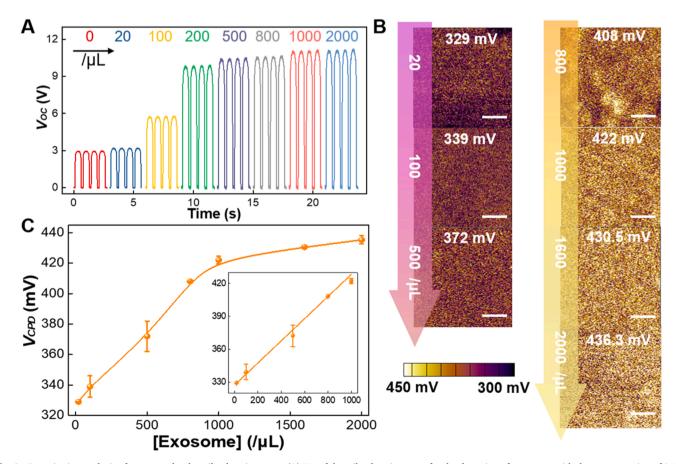
We have then investigated the variations of V_{oc} upon the introduction of different levels of exosomes. As shown in Fig. 2A, with the concentration of exosomes increased from 0 to 2000/μL, V_{oc} increases correspondingly. An obvious trend of contact potential difference can be observed. Two contact surfaces with a large difference in surface potential results in a large triboelectric charge [41]. To study the potential change of gold surface with the modification of TDNA and localization of target exosomes, we employ SKPM, which can give information about the electronic state of the local structures on the surface [42]. The contact potential difference (V_{CPD}) between the tip and sample is defined as [43]:

$$V_{CPD} = \frac{\varphi_{tip} - \varphi_{sample}}{-e} \tag{2}$$

where φ_{sample} and φ_{tip} are the work functions of the sample and the tip, and e is the electronic charge (1.60×10^{-19} C). Since the work function of the probe is constant, the level of work function can be compared by measuring surface potential difference. The higher the value of V_{CPD}, the smaller the work function of the sample is, that is, the easier it is to be positively charged during the contact electrification process [44]. The topographical images and surface potential maps in the presence of different levels of exosomes are listed in Fig. 2B. We have also established the relationship between V_{CPD} and the concentration of exosomes, as demonstrated in Fig. 2C. A linear equation ranging from 20 to 1000 /μL is fitted as follows:

$$y = 326·974 + 0.101\ x\ (n = 3, R^2 = 0.994) \tag{3}$$

in which y is the V_{CPD} (mV) and x is the concentration of target exosomes (/μL). The LOD is calculated to be 3 /μL on the basis of 3σ per slope, which is superior to that of the developed electrochemical sensor, demonstrating the advantages of triboelectric strategy as an excellent tool for monitoring target of interest. After comparing its analytical performances with recent representative exosome assays, this sensor shows the best LOD and relatively wide linear range (Table S2). Note that there is no signal amplification elements involved. The improved sensitivity can be attributed to the fact that exosomes contain an enormous number of amino groups which can generate significant triboelectric signal response even with extremely low concentration.

Fig. 2. Quantitative analysis of exosomes by the triboelectric sensor. (A) V_{oc} of the triboelectric sensor for the detection of exosomes with the concentration of 0, 20, 100, 200, 500, 800, 1000, 2000 /μL. (B) Surface charge potential images for the detection of exosomes with different concentrations (scale bars: 500 nm). (C) Calibration curve representing the relationship between the surface charge potential and the exosome concentration. Inset shows the linear range.

3.4. Triboelectric sensing mechanism

To further elaborate the contact electrification mechanism of this sensor, the charge transfer behavior between two different material surfaces and its corresponding energy band modification are studied. In this model, the electrons in the metal conform to the Fermi–Dirac distribution function [45]. In the ideal condition, the electrons will fill up all available energy states below the Fermi level (E_f), while the highest filled surface energy state of the dielectric is typically lower than the E_f of the metal. The topographical images and surface potential maps are shown in Fig. S6. After modified with TDNA, V_{CPD} increases from -175 to 75 mV. After further interacting with exosomes, a dramatical increase to 436.3 mV is achieved, which verify that SKPM is an excellent technique to monitor the step-by-step modifications and indicate the

existence of target exosomes. Based on these results and formula (2), the work function can be estimated to be approximately 4.85 eV and 4.49 eV in TDNA with and without exosomes, respectively.

For clearly explaining the contact electrification process of the triboelectric sensor, the surface state models are established. First, the Fermi level of gold appears very close to that of FEP, leading to the transfer of a small number of electrons from gold and FEP, resulting in the formation of a weak surface charge potential (Fig. 3A to C). Second, after TDNA embellishing on the gold surface, the E_f of the gold/TDNA gets a little rise, resulting in more charge transfer from the gold/TDNA surface to the FEP surface (Fig. 3D to F). Third, after the capture of exosomes by the aptamer sequence on the top of TDNA, more electrons incline to run on FEP surface state, which give the surface a higher tendency in generating positive triboelectric charges through the
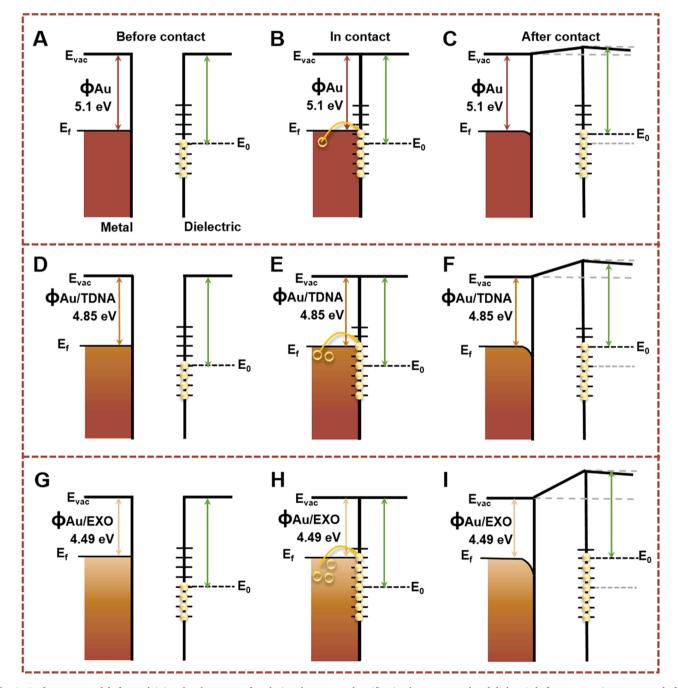

Fig. 3. Surface state models for explaining the charge transfers during the contact electrification between metal and dielectric before contact, in contact, and after contact: (A to C) between bare gold and dielectric; (D to F) between gold/TDNA and dielectric; (G to I) between gold/TDNA/exosome and dielectric.

contact electrification (Fig. 3G to I). Thus, exosomes with plenty of amino groups in the bases and amino acids largely enhance triboelectric charge density, compared with bare TDNA. This is mutually confirmed by the changes in outputs.

3.5. Demonstration of direct exosomes quantification in clinical samples

Finally, we have demonstrated the practical utility of this method by moving the system in biological circumstances. Different levels of exosomes from HeLa cells are firstly spiked in clinical human serum samples (10%). With the increase of added exosomes, the contact potential differences by SKPM have been measured. The concentration of exosomes can be calculated by referring to the formula (3) and the results are quite consistent with spiked values (Fig. 4). Since serum is a complicated biological system containing various biological molecules, it is concluded that this method can be a good candidate for exosome detection in real samples.

The capability of this method to distinguish different cell line-derived exosomes has been further investigated. We have cultured MCF-10A and Ramos cells as control cells to harvest exosomes. As shown in Fig. 5A, exosomes extracted from the three kinds of cells show similar saucer-like morphology in the TEM observations. However, it is reported that the expression levels of CD63 on the outer phospholipid bilayer of exosomes are different. We have performed western blot experiments to validate corresponding expressions levels (Fig. 5B). The band of HeLa exosomes is the thickest, indicating most abundant expression of CD63. On the contrary, the band of Ramos exosomes is the thinnest, demonstrating limited CD63 on the exosomes. The results are coinciding with previous reports [46]. Since CD63 is the key element for the capture of exosomes in the sensor, it is anticipated that these exosomes originated from different cell lines can be distinguished. We have then prepared the exosome samples with the same concentration and measured the

responses by the proposed sensor. As shown in Fig. 5C and D, HeLa cells result in the largest Q_{tr} and V_{CPD} values, while MCF-10A and Ramos cells contribute to the medium and low values. The results verify that with more CD63 on the surface, exosomes are more likely to be recognized by the aptamer on the top of TDNA and more intense signals can be achieved. As a result, excellent discriminant capability of this method towards specific exosomes is demonstrated.

4. Conclusion

In summary, a novel triboelectric sensor based on the modification of tetrahedral DNA is developed for capture and ultrasensitive determination of exosomes. With respect to previously developed methods, this work is unique in several attributes. First, 3-D DNA nanostructures are introduced in a TENG system for sensing purposes. The molecular layer is not only excellent electric conductor for touch isolation mode, but also acts as a selective target recognition element with enhanced capture efficacy. After interaction with exosomes, the contact area of top and bottom parts of TENG device is increased dramatically, which greatly improves TENG performances. This sensor achieves direct quantification and ultrahigh sensitivity even without any signal amplification. The LOD is as low as 3 exosomes/μL, which fulfills the requirements of most sensing applications. Second, due to the generated electricity by the TENG device, commercial LEDs could be lit up, which facilitates convenient and intuitive monitoring of exosomes. Third, the steps are simple and the whole detection is cost-effective and facile. Excellent practical utility is also confirmed by the experiments challenging different cells and clinical serum samples. Moreover, due to the relatively low structure complexity, it is anticipated that by changing the DNA sequences, most types of targets could be analyzed by this triboelectric sensing strategy. Therefore, we expect that the DNA nanostructures-assisted triboelectric sensor shows great prospect in
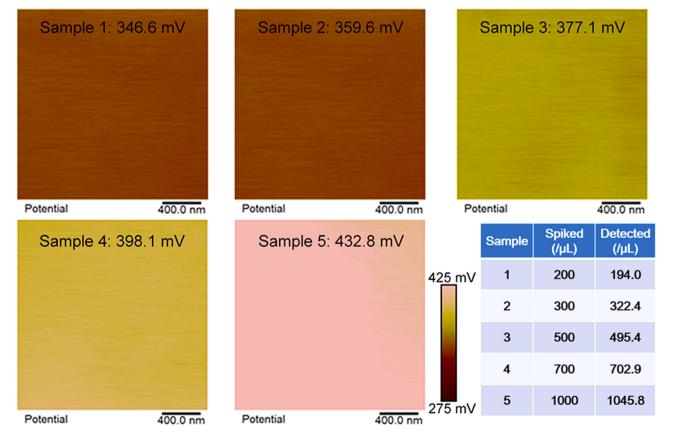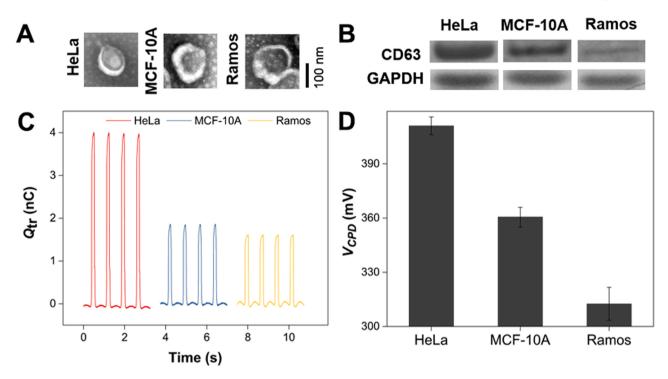

Sample	Spiked (/μL)	Detected (/μL)
1	200	194.0
2	300	322.4
3	500	495.4
4	700	702.9
5	1000	1045.8

Fig. 4. Surface charge potential images for the analysis of serum samples spiked with exosomes (200, 300, 500, 700, 1000 /μL) and the comparison of spiked values and calculated values.

Fig. 5. Analysis of exosomes from different cell lines. (A) TEM images of exosomes extracted from HeLa, MCF-10A and Ramos cells. (B) Western blot bands of CD63 in different exosomes. (C) Q_{tr} of the triboelectric sensor for the analysis of exosomes from HeLa, MCF-10A and Ramos cells. (D) Histogram of surface charge potential of the above samples. Error bars represent standard deviations of four independent measurements.

biological and analytical applications.

CRediT authorship contribution statement

P.M., Z.W. and Z.L.W. conceived the idea. L.J.X. and Z.W. led the mechanical modeling and theoretical studies. P.M. X.Y.M. and Y.G.T. performed electrical measurements and analyzed the data. P.M., X.H.S., W.Z. and Z.L.W. prepared the manuscript.

Declaration of Competing Interest

The authors declare that they have no known competing financial interests or personal relationships that could have appeared to influence the work reported in this paper.

Appendix A. Supporting information

Supplementary data associated with this article can be found in the online version at doi:10.1016/j.nanoen.2021.106781.

References

[1] K. Trajkovic, C. Hsu, S. Chiantia, L. Rajendran, D. Wenzel, F. Wieland, P. Schwille, B. Brügger, M. Simons, Ceramide triggers budding of exosome vesicles into multivesicular endosomes, Science 319 (2008) 1244–1247.

[2] C.J. He, S. Zheng, Y. Luo, B. Wang, Exosome theranostics: biology and translational medicine, Theranostics 8 (2018) 237–255.

[3] N. Yim, S.W. Ryu, K. Choi, K.R. Lee, S. Lee, H. Choi, J. Kim, M.R. Shaker, W. Sun, J. H. Park, D. Kim, W.D. Heo, C. Choi, Exosome engineering for efficient intracellular delivery of soluble proteins using optically reversible protein-protein interaction module, Nat. Commun. 7 (2016) 12277.

[4] J. Wang, B.Z. Yeung, M.J. Cui, C.J. Peer, Z. Lu, W.D. Figg, M.G. Wientjes, S. Woo, J. L.S. Au, Exosome is a mechanism of intercellular drug transfer: application of quantitative pharmacology, J. Control. Release 268 (2017) 147–158.

[5] L. Song, S. Tang, X.L. Han, Z.Y. Jiang, L.L. Dong, C.C. Liu, X.Y. Liang, J.X. Dong, C. X. Qiu, Y.X. Wang, Y.F. Du, KIBRA controls exosome secretion via inhibiting the proteasomal degradation of Rab27a, Nat. Commun. 10 (2019) 1639.

[6] H.O. Yang, H.Y. Zhang, S.H. Ge, T. Ning, M. Bai, J.L. Li, S. Li, W. Sun, T. Deng, L. Zhang, G.G. Ying, Y. Ba, Exosome-derived miR-130a activates angiogenesis in gastric cancer by targeting C-MYB in vascular endothelial cells, Mol. Ther. 26 (2018) 2466–2475.

[7] N. Jiang, L.S. Xiang, L. He, G.D. Yang, J.X. Zhen, C.L. Wang, Y.M. Zhang, S. N. Wang, Y. Zhou, T.J. Sheu, J.Q. Wu, K.N. Chen, P.G. Coelho, N.M. Tovar, S. H. Kim, M. Chen, Y.H. Zhou, J.J. Mao, Exosomes mediate epithelium-mesenchyme crosstalk in organ development, ACS Nano 11 (2017) 7736–7746.

[8] M.K.S. Tang, P.Y.K. Yue, P.P. Ip, R.L. Huang, H.C. Lai, A.N.Y. Cheung, K.Y. Tse, H. Y.S. Ngan, A.S.T. Wong, Soluble E-cadherin promotes tumor angiogenesis and localizes to exosome surface, Nat. Commun. 9 (2018) 2270.

[9] A. Hoshino, B. Costa-Silva, T.-L. Shen, G. Rodrigues, A. Hashimoto, M. Tesic Mark, H. Molina, S. Kohsaka, A. Di Giannatale, S. Ceder, S. Singh, C. Williams, N. Soplop, K. Uryu, L. Pharmer, T. King, L. Bojmar, A.E. Davies, Y. Ararso, T. Zhang, H. Zhang, J. Hernandez, J.M. Weiss, V.D. Dumont-Cole, K. Kramer, L.H. Wexler, A. Narendran, G.K. Schwartz, J.H. Healey, P. Sandstrom, K. Jørgen Labori, E. H. Kure, P.M. Grandgenett, M.A. Hollingsworth, M. de Sousa, S. Kaur, M. Jain, K. Mallya, S.K. Batra, W.R. Jarnagin, M.S. Brady, O. Fodstad, V. Muller, K. Pantel, A.J. Minn, M.J. Bissell, B.A. Garcia, Y. Kang, V.K. Rajasekhar, C.M. Ghajar, I. Matei, H. Peinado, J. Bromberg, D. Lyden, Tumour exosome integrins determine organotropic metastasis, Nature 527 (2015) 329–335.

[10] M.D. Keller, K.L. Ching, F.X. Liang, A. Dhabaria, K. Tam, B.M. Ueberheide, D. Unutmaz, V.J. Torres, K. Cadwell, Decoy exosomes provide protection against bacterial toxins, Nature 579 (2020) 260–264.

[11] H. Choi, Y. Kim, A. Mirzaaghasi, J. Heo, Y.N. Kim, J.H. Shin, S. Kim, N.H. Kim, E. S. Cho, J.I. Yook, T.H. Yoo, E. Song, P. Kim, E.C. Shin, K. Chung, K. Choi, C. Choi, Exosome-based delivery of super-repressor I kappa B alpha relieves sepsis-associated organ damage and mortality, Sci. Adv. 6 (2020) eaaz6980.

[12] C.C. Liu, X.N. Xu, B. Li, B. Situ, W.L. Pan, Y. Hu, T.X. An, S.H. Yao, L. Zheng, Single-exosome-counting immunoassays for cancer diagnostics, Nano Lett. 18 (2018) 4226–4232.

[13] Y. Lyu, D. Cui, J.G. Huang, W.X. Fan, Y.S. Miao, K.Y. Pu, Near-infrared afterglow semiconducting nano-polycomplexes for the multiplex differentiation of cancer exosomes, Angew. Chem., Int. Ed. 58 (2019) 4983–4987.

[14] X.N. Fang, Y.K. Duan, G.B. Adkins, S.Q. Pan, H. Wang, Y. Liu, W.W. Zhong, Highly efficient exosome isolation and protein analysis by an integrated nanomaterial-based platform, Anal. Chem. 90 (2018) 2787–2795.

[15] Z.G. Yang, J. Xie, J. Zhu, C. Kang, C.L. Chiang, X.M. Wang, X.B. Wang, T.R. Kuang, F. Chen, Z. Chen, A.L. Zhang, B. Yu, R.J. Lee, L.S. Teng, L.J. Lee, Functional exosome-mimic for delivery of siRNA to cancer: in vitro and in vivo evaluation, J. Control. Release 243 (2016) 160–171.

[16] D. He, L. Hai, H. Wang, R. Wu, H.W. Li, Enzyme-free quantification of exosomal microRNA by the target-triggered assembly of the polymer DNAzyme nanostructure, Analyst 143 (2018) 813–816.

[17] M. Paulaitis, K. Agarwal, P. Nana-Sinkam, Dynamic scaling of exosome sizes, Langmuir 34 (2018) 9387–9393.

[18] W. Anderson, R. Lane, D. Korbie, M. Trau, Observations of tunable resistive pulse sensing for exosome analysis: improving system sensitivity and stability, Langmuir 31 (2015) 6577–6587.

[19] R. Hinchet, H.J. Yoon, H. Ryu, M.K. Kim, E.K. Choi, D.S. Kim, S.W. Kim, Transcutaneous ultrasound energy harvesting using capacitive triboelectric technology, Science 365 (2019) 491–494.

[20] C. Chen, Z. Wen, A.M. Wei, X.K. Xie, N.N. Zhai, X.L. Wei, M.F. Peng, Y.N. Liu, X. H. Sun, J.T.W. Yeow, Self-powered on-line ion concentration monitor in water transportation driven by triboelectric nanogenerator, Nano Energy 62 (2019) 442–448.

[21] Z. Wen, Y.Q. Yang, N. Sun, G.F. Li, Y.N. Liu, C. Chen, J.H. Shi, L.J. Xie, H.X. Jiang, D.Q. Bao, Q.Q. Zhuo, X.H. Sun, A wrinkled PEDOT:PSS film based stretchable and transparent triboelectric nanogenerator for wearable energy harvesters and active motion sensors, Adv. Funct. Mater. 28 (2018) 1803684.

[22] Y. Xi, J. Wang, Y.L. Zi, X.G. Li, C.B. Han, X. Cao, C.G. Hu, Z.L. Wang, High efficient harvesting of underwater ultrasonic wave energy by triboelectric nanogenerator, Nano Energy 38 (2017) 101–108.

[23] Y.K. Jung, K.N. Kim, J.M. Baik, B.S. Kim, Self-powered triboelectric aptasensor for label-free highly specific thrombin detection, Nano Energy 30 (2016) 77–83.

[24] J.H. Wang, H. Wang, T.Y.Y. He, B.R. He, N.V. Thakor, C. Lee, Investigation of low-current direct stimulation for rehabilitation treatment related to muscle function loss using self-powered TENG system, Adv. Sci. 6 (2019) 1900149.

[25] J.Q. Xiong, H.S. Luo, D.C. Gao, X.R. Zhou, P. Cui, G. Thangavel, K. Parida, P.S. Lee, Self-restoring, waterproof, tunable microstructural shape memory triboelectric nanogenerator for self-powered water temperature sensor, Nano Energy 61 (2019) 584–593.

[26] X. Wang, A.R. Chandrasekaran, Z.Y. Shen, Y.P. Ohayon, T. Wang, M.E. Kizer, R. J. Sha, C.D. Mao, H. Yan, X.P. Zhang, S.P. Liao, B.Q. Ding, B. Chakraborty, N. Jonoska, D. Niu, H.Z. Gu, J. Chao, X. Gao, Y.H. Li, T. Ciengshin, N.C. Seeman, Paranemic crossover DNA: there and back again, Chem. Rev. 119 (2019) 6273–6289.

[27] H. Chai, P. Miao, Bipedal DNA walker based electrochemical genosensing strategy, Anal. Chem. 91 (2019) 4953–4957.

[28] Z.L. Ge, Z.M. Su, C.R. Simmons, J. Li, S.X. Jiang, W. Li, Y. Yang, Y. Liu, W. Chiu, C. H. Fan, H. Yan, Redox engineering of cytochrome c using DNA nanostructure-based charged encapsulation and spatial control, ACS Appl. Mater. Interfaces 11 (2019) 13874–13880.

[29] S. Wang, L.Q. Zhang, S. Wan, S. Cansiz, C. Cui, Y. Liu, R. Cai, C.Y. Hong, I.T. Teng, M.L. Shi, Y. Wu, Y.Y. Dong, W.H. Tan, Aptasensor with expanded nucleotide using DNA nanotetrahedra for electrochemical detection of cancerous exosomes, ACS Nano 11 (2017) 3943–3949.

[30] P. Miao, B.D. Wang, X.F. Chen, X.X. Li, Y.G. Tang, Tetrahedral DNA nanostructure-based microRNA biosensor coupled with catalytic recycling of the analyte, ACS Appl. Mater. Interfaces 7 (2015) 6238–6243.

[31] J. Wang, F.Y. Cheng, F.Y. Meng, M. Yang, Y. Pan, P. Miao, Hand-in-hand RNA nanowire-based aptasensor for the detection of theophylline, Biosens. Bioelectron. 101 (2018) 153–158.

[32] C. Li, X.L. Hu, J.Y. Lu, X.X. Mao, Y. Xiang, Y.Q. Shu, G.X. Li, Design of DNA nanostructure-based interfacial probes for the electrochemical detection of nucleic acids directly in whole blood, Chem. Sci. 9 (2018) 979–984.

[33] M. Hou, D.G. He, H.C. Bu, H.Z. Wang, J. Huang, J.Q. Gu, R. Wu, H.W. Li, X.X. He, K.M. Wang, A sandwich-type surface-enhanced Raman scattering sensor using dual aptamers and gold nanoparticles for the detection of tumor extracellular vesicles, Analyst 145 (2020) 6232–6236.

[34] H.Z. Wang, K.J. Wan, Y. Zhou, X.X. He, D.G. He, H. Cheng, J. Huang, R.C. Jia, K. M. Wang, A three-dimensional multipedal DNA walker for the ultrasensitive detection of tumor exosomes, Chem. Commun. 56 (2020) 12949–12952.

[35] D.G. He, S.L. Ho, H.N. Chan, H.Z. Wang, L. Hai, X.X. He, K.M. Wang, H.W. Li, Molecular-recognition-based DNA nanodevices for enhancing the direct visualization and quantification of single vesicles of tumor exosomes in plasma microsamples, Anal. Chem. 91 (2019) 2768–2775.

[36] D.G. He, H.Z. Wang, S.E.L. Ho, H.G. Chan, L. Hai, X.X. He, K.M. Wang, H. Li, Total internal reflection-based single-vesicle in situ quantitative and stoichiometric analysis of tumor-derived exosomal microRNAs for diagnosis and treatment monitoring, Theranostics 9 (2019) 4494–4507.

[37] X.Y. Ma, P. Miao, Silver nanoparticle@DNA tetrahedron-based colorimetric detection of HIV-related DNA with cascade strand displacement amplification, J. Mater. Chem. B 7 (2019) 2608–2612.

[38] C.Y. Jiang, F.Y. Meng, D.S. Mao, Y.G. Tang, P. Miao, Tetrahedral DNA nanoconjugates for simultaneous measurement of telomerase activity and miRNA, Chembiochem 22 (2021) 1302–1306.

[39] T. Charoonsuk, S. Pongampai, P. Pakawanit, N. Vittayakorn, Achieving a highly efficient chitosan-based triboelectric nanogenerator via adding organic proteins: influence of morphology and molecular structure, Nano Energy 89 (2021), 106430.

[40] S.H. Wang, Y.L. Zi, Y.S. Zhou, S.M. Li, F.R. Fan, L. Lin, Z.L. Wang, Molecular surface functionalization to enhance the power output of triboelectric nanogenerators, J. Mater. Chem. A 4 (2016) 3728–3734.

[41] W. Seung, H.J. Yoon, T.Y. Kim, H. Ryu, J. Kim, J.H. Lee, J.H. Lee, S. Kim, Y.K. Park, Y.J. Park, S.W. Kim, Boosting power-generating performance of triboelectric nanogenerators via artificial control of ferroelectric polarization and dielectric properties, Adv. Energy Mater. 7 (2017) 1600988.

[42] T. Glatzel, S. Sadewasser, R. Shikler, Y. Rosenwaks, M.C. Lux-Steiner, Kelvin probe force microscopy on III-V semiconductors: the effect of surface defects on the local work function, Mater. Sci. Eng.: B 102 (2003) 138–142.

[43] W. Melitz, J. Shen, A.C. Kummel, S. Lee, Kelvin probe force microscopy and its application, Surf. Sci. Rep. 66 (2011) 1–27.

[44] J.W. Lee, H.J. Cho, J. Chun, K.N. Kim, S. Kim, C.W. Ahn, I.W. Kim, J.Y. Kim, S. W. Kim, C. Yang, J.M. Baik, Robust nanogenerators based on graft copolymers via control of dielectrics for remarkable output power enhancement, Sci. Adv. 3 (2017), e1602902.

[45] N.D. Lang, W. Kohn, Theory of metal surfaces – work function, Phys. Rev. B 3 (1971) 1215–1223.

[46] Q.M. Feng, P. Ma, Q.H. Cao, Y.H. Guo, J.J. Xu, An aptamer-binding DNA walking machine for sensitive electrochemiluminescence detection of tumor exosomes, Chem. Commun. 56 (2020) 269–272.